Journal of Photochemistry and Photobiology A: Chemistry 339 (2017) 95–102

Contents lists available at ScienceDirect

Journal of Photochemistry and Photobiology A: Chemistry

journal homepage: www.elsevier.com/locate/jphotochem

Charge transfer mechanism of WO_3/TiO_2 heterostructure for photoelectrochemical water splitting

I.A. Castro[a,*], G. Byzynski[b], M. Dawson[c], C. Ribeiro[d]

[a] Chemistry Department, Federal University of São Carlos, São Carlos, SP, Brazil
[b] Chemistry Department, Sao Paulo State University, UNESP, Araraquara, SP, Brazil
[c] Materials Science and Engineering Department, Federal University of São Carlos, São Carlos, SP, Brazil
[d] Embrapa Instrumentation, São Carlos, SP, Brazil

ARTICLE INFO

Article history:
Received 10 November 2016
Received in revised form 11 February 2017
Accepted 26 February 2017
Available online 28 February 2017

Keywords:
Electron-hole pairs
Hole scavenger
Charge recombination
Tungsten oxide
Titanium oxide
Heterostructure
Band edge manipulation

ABSTRACT

The present study shows how electronic parameters (e.g. band gap energy, band edge positions) on semiconductors affect photoelectrochemical activity in simulated solar light using WO_3, TiO_2 and WO_3/TiO_2 as model systems. Hydrothermal synthesis was conducted to study heterostructure (HE) formation, which the loading of WO_3 in TiO_2 structure were varied to 20, 40 and 80 wt%. Scanning electron microscopy images show that WO_3 and TiO_2 particles are in contact with each other and the synthesis method as well as the deposition method are appropriate for the formation of WO_3/TiO_2 HE film. Important findings were obtained with a hole scavenger during photoelectrochemical characterization of WO_3/TiO_2–40 wt% film. This strategy was effective to clearly distinguish charge transport from charge separation, the essential mechanisms that affect water splitting which are often misinterpreted experimentally for HE. The hole scavenger experiment depicts the increase by 17.5% in photocurrent density for the WO_3/TiO_2–40 wt% film as compared to WO_3 film, corresponding to 210 and 12 $\mu A\,cm^{-2}$ vs Ag/AgCl respectively. Additionally, this HE film showed water oxidation initiated at lower applied potentials and indicating that coupling of the materials resulted in optimization of band edge properties for water splitting with the increase on light absorption at the visible range. Flat band potential was determined by the Mott-Schottky plot and it indicated the difference of 1.08 V vs Ag/AgCl between TiO_2 and WO_3 potentials, which makes the charge injection from one structure to another effective and thermodynamically stable for charge separation. A charge carrier density of 1.59×10^{20} was observed for the WO_3/TiO_2–40 wt% and it supports the best photoelectrochemical performance for water oxidation.

1. Introduction

TiO_2 based catalysts have been extensively investigated for photocatalytic applications. Since the pioneering study of Fujishima and Honda in the early 1970s, where the authors reported water splitting in a photoelectrochemical cell illuminated with near ultraviolet light using TiO_2 as a photoelectrode, several works have been motivated by the promising properties of TiO_2 [1,2]. Despite the advantages associated with the use of TiO_2 such as low cost, nontoxicity and high stability, this oxide suffers from poor utilization of the solar spectrum (band gap energy for anatase crystalline phase is 3.2 eV; ~390 nm) and as a result it makes use of only 2.5–3.5% of the solar light that reaches the Earth [3–6].

In recent literature, significant investigations are underway regarding the optimization of TiO_2 and also the coupling of TiO_2 with other semiconductors (heterostructures or heterojunctions) that present absorption beyond the UV region, in order to improve the light absorption of TiO_2 in the visible regions of sunlight [3,7–9]. These investigations aim to identify the phenomena that occur at the crystalline interface, such as Fermi level alignment, and the influence of band edges (valence and conduction bands) on photocatalytic activity [10–12].

In this context, transition metal compounds, especially tungsten oxide (WO_3), are an abundant material with promising potential for many technological applications. WO_3 presents unique optical and electronic properties that can be explored for the development of a series of functional structural phases [13,14]. To date, WO_3 photoanodes produced by hydrothermal synthesis show high chemical and thermo stability. However, for practical application the photoanodes are still needed best performance for

* Corresponding author.
E-mail address: isacastro25@gmail.com (I.A. Castro).

http://dx.doi.org/10.1016/j.jphotochem.2017.02.024
1010-6030/

photoelectric conversion [15]. In order to improve the performance of TiO_2, the coupling of low band gap materials such as WO_3 with TiO_2 to form heterostructures is one of the most important approaches to band gap engineering, which can enhance photocatalytical or photoelectrocatalytical properties at the visible region [16,17,12,4].

The key parameters for better understanding and optimization of the photocatalytic performance of semiconductors is the determination of their band edge positions [18]. It is well known that the band gap positions and Fermi level energy play important roles in allowing electron transfer in heterostructured systems. Thus, the knowledge derived from energy diagram scans open a window for the characterization of the processes that take place at the surface of semiconductor materials. In this context, photoelectrochemical measurements are ideal techniques that can provide information about the intrinsic electronic properties of semiconductors in contact with electrolyte solutions [19,18]. Several papers describe the development of new catalysts for different applications, but there is a need for further understanding of the main active species and mechanisms for effective water splitting [15].

Several reports have shown the growth of heterostructures using hydrothermal annealing with controlled morphology and crystallinity [20–23]. The observed alignment at the contact interface of semiconductor oxides may be a good strategy for tailoring heterostructures for the study of the charge transfer mechanism for the photoelectrochemical water splitting.

The present study aims to investigate how the electronic parameters (band edge positions, Fermi level energy and charge migration) affect the photocatalytic activity of heterostructures obtained by hydrothermal synthesis. The as-synthesized materials will be investigated with current-voltage measurements. This work is expected to assist the comprehension of the photochemical mechanism that occurs at the heterostructure interface in order to optimize the material's electronic properties for photocatalytic applications.

2. Experimental

2.1. Material synthesis

In a typical synthesis procedure, 0.12 mol L^{-1} solution was prepared by dissolving precursor tungstic acid – H_2WO_4 (Aldrich, 99%) in H_2O_2 (Synth, 29%), to form a stable peroxo-polytungstic acid solution at room temperature. Subsequently, hydrothermal synthesis was conducted to produce the heterostructures where TiO_2 nanopowder (Aldrich, 99.7%) was used as a pre-formed particle to obtain heterostructures utilizing stable peroxo-polytungstic acid solution. The necessary mass of W in the peroxo-complex solution to obtain heterostructures with 20, 40 and 80 wt % of W was calculated.

The solution was placed into a 100 mL micro-controlled hydrothermal cell, which had fine control of temperature and monitoring of the self-generated pressure. The precursors were subjected to hydrothermal treatment at 200 °C under magnetic stirring for 24 h. The same procedure was performed without TiO_2, to obtain only WO_3 particles and for the purpose of checking the properties of the oxide as a comparison of WO_3 with the as-synthesized heterostructures. All materials were separated by centrifugation and dried at 80 °C for 12 h. A summarized denomination of each material is presented in Table 1.

Thin films were produced using the pre-formed oxides and the heterostructures. The paste was prepared for each material by adding 2.67 mL of terpineol (Aldrich) and 3.33 mL of ethyl cellulose solution (Aldrich, 46 cP, 5% in toluene/ethanol 80:20) 10% in pure ethanol (99.9%) and then mixing to obtain a homogenous mixture for film production. The as-prepared homogenous paste was dropped onto the fluorine doped SnO_2 (FTO) substrate and spin-coated for film deposition and to remove residual precursor solution.

Table 1
Synthesized materials W-peroxo/TiO_2 with varying W (mass wt%).

Samples	(W-peroxo/TiO_2)
Commercial TiO_2	0/100
WO_3	100/0
WO_3/TiO_2–20 wt%	20/80
WO_3/TiO_2–40 wt%	40/60
WO_3/TiO_2–80 wt%	80/20

2.2. Material characterization

Sample morphology was characterized via field emission scanning electron microscopy (FE-SEM, JEOL JSM 6701F) and energy-dispersive X-ray spectroscopy (EDX) (JEOL SEM 6310 microscope) to evaluate the homogeneity, WO_3 and TiO_2 distribution, and surface quality. X-ray diffraction (XRD) analysis was performed with a Shimadzu XRD 6000 with radiation at 1.5456 Å, which corresponds to Cu kα emission, at a step scan of 0.02° and exposure time of 4 s. The UV–vis spectra were acquired using a Spectrophotometer Cary 5G (Varian) in the diffuse reflectance mode (DRS).

2.3. Photoelectrocatalytic activity

Electrochemical measurements were carried out in a conventional three-electrode system, connected to a computer-controlled potentiostat (Autolab PGSTAT 302 N, Metrohm-Eco Chemie controlled by GPES software). The three-electrode system contained thin films as the working-electrode, a Pt wire as the counter-electrode, and Ag/AgCl as the reference electrode. The photoelectrocatalytic activity was measured using simulated solar irradiation 500 W Xenon (Newport, 66902) calibrated to 100 mW cm^{-2} and air mass 1.0 global (AM 1.0G) filter.

Linear Sweep Voltammetry (LSV) was carried out using 0.5 mol L^{-1} aqueous solution of Na_2SO_4 pH 5at 0.5 m V s^{-1} with potential range of −0.5 to 1.2 vs Ag/AgCl. Every measurement was repeated three times to ensure equilibrium. In the results section, only the third voltammogram is presented for every measurement. Mott-Schottky plots were obtained at a frequency range of 5–10 kHz, amplitude of 10 mV, in the potential range of −1.0 to 1.0 V vs Ag/AgCl. The Mott-Schottky equation was applied to investigate the flat band potential (E_{FB}) of the electrodes as described elsewhere [19].

3. Results and discussion

The morphology of the as-prepared powders was investigated by SEM images, as shown in Fig. 1.

The heterostructures and the precursor oxides showed different particle morphologies. Pristine WO_3 showed the presence of micro-aggregates in a three-dimensional structure (Fig. 1a) and TiO_2 presented smaller particles at nanometer range (Fig. 1b), formed by agglomerates. For the heterostructures, the presence of micro-aggregates was observed, which is characteristic of WO_3 particles, while smaller particles with spherical and agglomerated morphology possibly correspond to TiO_2. Importantly, SEM images show that WO_3 and TiO_2 particles are in contact with each other and can be indicative of attachment due to the hydrothermal conditions utilized, as indicated in Fig. 1d. Since the hydrothermal method can induce collisions among crystallized particles, under

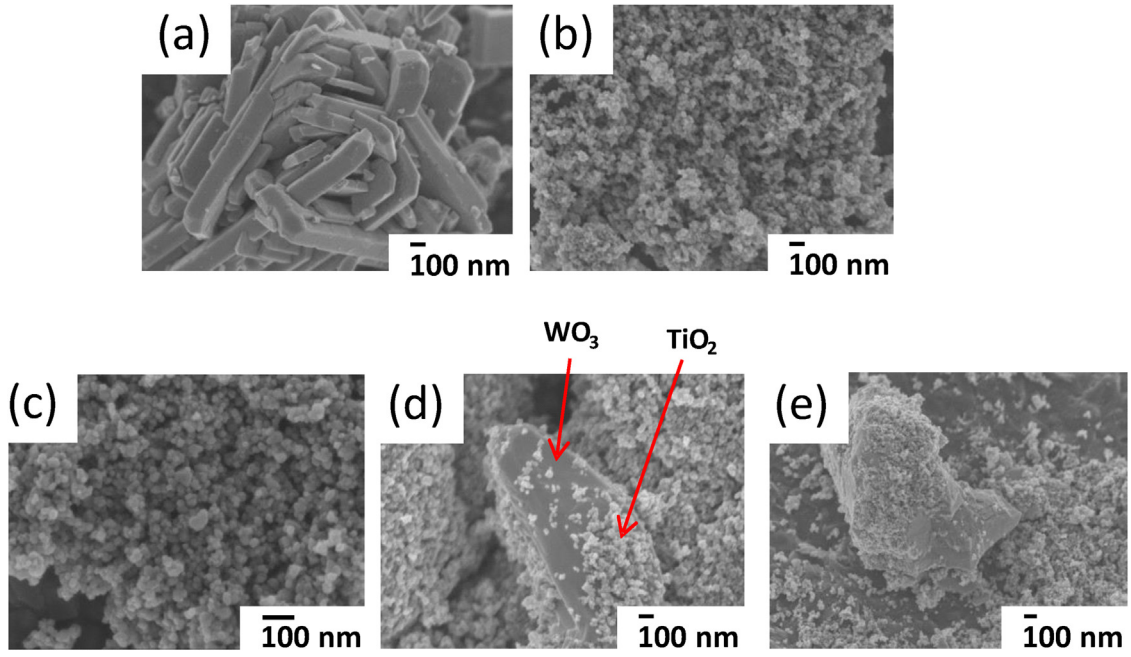

Fig. 1. FE-SEM images of WO_3 (a), TiO_2 (b), WO_3/TiO_2–20 wt% (c), WO_3/TiO_2–40 wt% (d) and WO_3/TiO_2–80 wt% (e).

high pressure and temperature, it is possible to infer that the heterostructures were successfully produced.

With respect to WO_3/TiO_2–80 wt%, EDX mapping was carried out to confirm the presence of WO_3 and TiO_2 particles in this heterostructured system. As seen in Supplementary Fig. 1, the particles for both 40 wt% and 80 wt% presented particles in the micrometer range that is correspondent to WO_3 with plate-like morphology. The regions with the nanoparticulated agglomerates could be associated to TiO_2. It is possible to conclude that the heterostructures were formed by the crystallization of WO_3 micro-particles attached to TiO_2 nanoparticulated agglomerates. Since TiO_2 was used as a pre-formed particle during the hydrothermal synthesis, it is expected that the WO_3 micro-particles crystallize in contact with the pre-formed TiO_2 as a crystalline template.

Since film samples are necessary for the proposed electrochemical characterization experiments, the calcination step (necessary for particle adherence on FTO substrate) may change morphology and, consequently, general properties. The microstructures of the calcined films are presented in Fig. 2. The discrepancy in particle size and morphology between WO_3 and TiO_2 is evident. The micrograph of TiO_2 shows agglomerates formed of uniform spherical particles of approximately 40 nm (Fig. 2a) while WO_3 microstructure consists of agglomerates of large irregularly shaped particles. WO_3/TiO_2–40 wt% film presents small particles believed to be TiO_2 on top of large irregularly shaped particles believed to be WO_3 due to the sizes of pristine TiO_2 and WO_3. An important aspect is the similar particle size, mainly of the heterostructure film (Fig. 2c) when compared to the freestanding particles. This reveals that the calcination procedure was not enough to promote significant grain growth, which confirms that the synthesis and film preparation methods are adequate for the proposed study. EDX elemental spectra of WO_3/TiO_2–40 wt% film shows elemental composition of Ti and W (Supplementary Fig. 2). Sn detection is associated with the FTO substrate. Further, the elemental maps show uniform distribution of Ti and W in the film, an indication that the synthesis method as well as the deposition method are appropriate for the formation of WO_3:TiO_2 heterostructures (Suppl. Fig. 2b and c).

However, the film preparation procedure was shown as influential on phase composition of heterostructures. Fig. 3a presents XRD patterns for the pristine oxides (TiO_2 and WO_3) and the heterostructures (20 wt%, 40 wt% and 80 wt%).

The crystallographic properties of as-synthesized powders were determined by XRD measurements (Fig. 3a). The orthorhombic phase of $WO_3{\cdot}0.33H_2O$ (JPDS N° 35-0270) was identified as the principal phase for the pristine WO_3 sample with WO_3 planes showed in Fig. 3a. The main WO_3 orthorhombic phase is (002) and (220) planes, similar presented by Li et al. [24]. They obtained diverse micro to nanostructures of WO_3 orthorhombic crystallites through microwave heating under different conditions. The anatase phase of TiO_2 (JPDS N° 01-086-1157) was identified as the main crystallographic phase in the TiO_2 nanoparticle sample

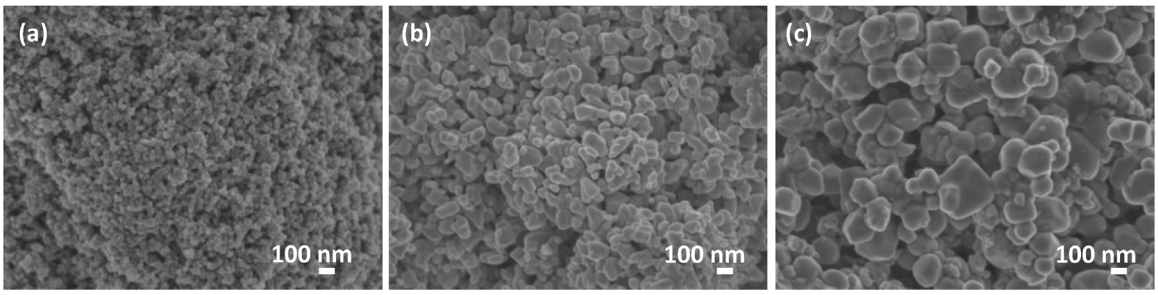

Fig. 2. FE-SEM images of films (a) TiO_2 (b) WO_3 and (c) WO_3/TiO_2–40 wt%.

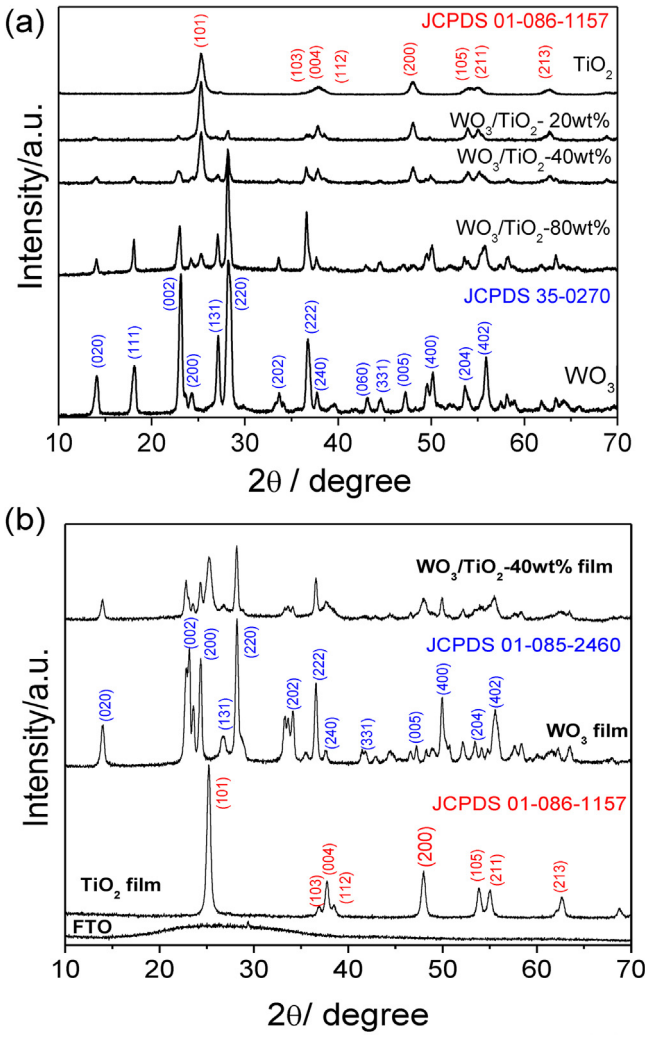

Fig. 3. XRD patterns of powder samples (a) and the films (b). Main peaks are labelled for TiO_2 and WO_3 crystal planes with corresponedent JCPDS card numebers.

(Fig. 3A). The diffraction peak in 25.35°; 36.07°; 37.80°; 40.90°; 54.11°; 62.73° correspond to the (101), (103), (004), (112), (200), (105), (211), and (213) crystal planes of the anatase phase, respectively.

The powder heterostructures exhibit TiO_2 anatase phase peaks (JCPDS N° 01-086-1157) and $WO_3{\cdot}0.33H_2O$ orthorhombic phase peaks (JCPDS N° 35-0270) as the main crystalline phases. The powder heterostructures exhibit XRD patterns correspondent to TiO_2 anatase (JCPDS N° 01-086-1157) and $WO_3{\cdot}0.33H_2O$ orthorhombic (JCPDS N° 35-0270) as the main crystalline phases. The intensity of the (101) antase TiO_2 plane is reduced with W loading and it may indicates the preferential WO_3 attachment at TiO_2 (101) crystal orientation to obtain the heterostructures.

Fig. 3b shows XRD patterns for the produced films deposited over the FTO substrate. As one can see, crystalline phase was not changed after TiO_2 film. However, during calcination, WO_3 changed from orthorhombic structure to hexagonal, as confirmed by JCPDS N° 01-085-2460. Ramana et al. [25] confirms that the WO_3 phase transitions in thin films occur as the temperature increases, starting as monoclinic phase, then orthorhombic phase at 350 °C and, finally, hexagonal phase at 500 °C. There is no evidence of heterostructure detachment, i.e., by SEM images it is possible to assume that the heterostructure was preserved even after the WO_3 phase modification.

WO_3/TiO_2–40 wt% corresponds to the best performance composition expected, as based on recent reports [20,21], and it is a representative material to evidence the heterojunction effect on semiconductor properties. It is well known that heteroaggregation process is driven by collisions between different nanoparticles during hydrothermal annealing and it was studied for different semiconductor oxide models in our research group. [20,21], The best composition was chosen based on these recent publications and considering FE-SEM images of WO_3/TiO_2 40 wt% with the indication of heterostucture formation in Fig. 1d for further characterization.

The electronic structure of the films was investigated using UV–vis spectra in reflectance mode. The indirect transition model was used to estimate the band gap energy (E_g) of the semiconductors by Tauc equation [20] and it is presented in Fig. 4.

TiO_2 film showed an absorption edge at 380 nm and a band gap of 3.26 eV, which is in agreement with its band gap energy reported in literature with a characteristic absorption in the UV region of the spectrum [2]. For WO_3 film, the band gap energy is observed at 3.03 eV and equivalent to 409 nm, thus the light absorption is extend for photocatalytic reactions. The WO_3/TiO_2–40 wt% film presented intermediate band gap energy between pristine TiO_2 and WO_3 values (3.23 eV). Also, FTO substrate presented a band gap energy at 3.36 eV and one can see that it is not an interference at the estimated band gap for the as-prepared films.

4. Photoelectrochemical characterization

The photoelectrocatalytic performance of the produced films was investigated for water oxidation as shown in Fig. 5a. The LSV characteristics under dark and under simulated solar irradiation at 50 mV s^{-1} is shown, using the produced films and Na_2SO_4 0.5 mol L^{-1}. A summary of the results is presented in Table 2.

The films presented no significant current in dark conditions, in the potential range from −0.5 to 1.2 V (vs Ag/AgCl reference electrode) and the higher current density observed is of WO_3/TiO_2 film but it still negligible compared to the data collected under illumination. With simulated solar irradiation, the current reached 29.5 μA cm^{-2} for WO_3 film at 0.75 V vs Ag/AgCl. On the other hand, TiO_2 film current does not deviate from zero significantly. This is expected since the band gap energy observed for TiO_2 film is in the order of UV region (3.26 eV).

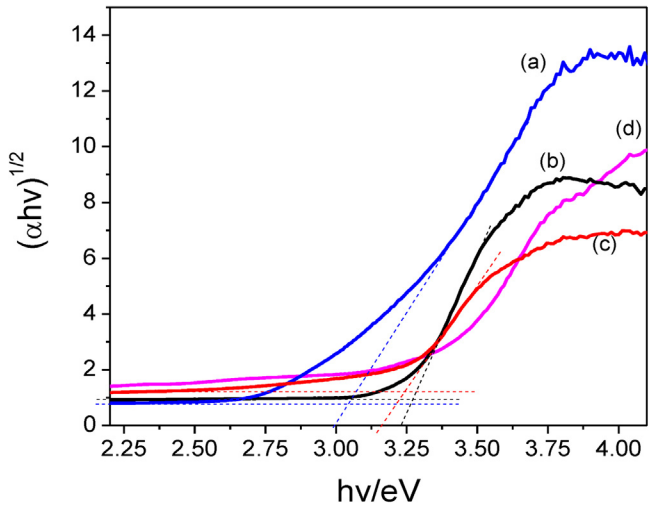

Fig. 4. UV–vis diffuse reflectance spectra of the (a) WO_3 film, (b) TiO_2 film, (c) WO_3/TiO_2–40 wt% film and (d) FTO substrate. The intersection between the horizontal and vertical short dash dotted curves are the reference value of estimated E_g for the films.

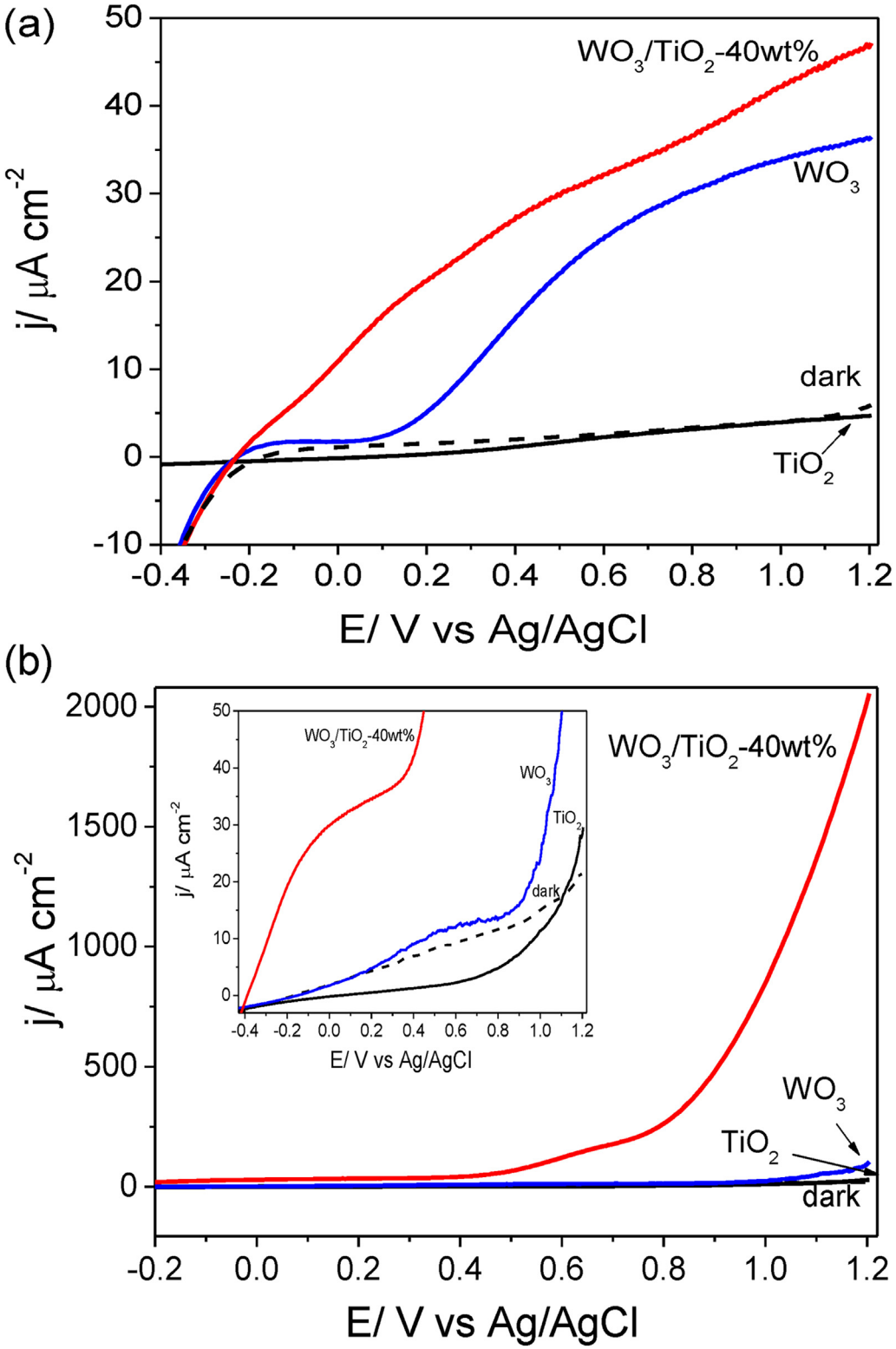

Fig. 5. (a) LSV characteristics obtained of the produced films at 50 mV s^{-1} in Na_2SO_4 0.5 mol L^{-1} electrolyte and (b) in Na_2SO_3 0.5 mol L^{-1} + Na_2SO_4 0.5 mol L^{-1} electrolyte. Insert: expanded view of Fig. 5b equivalent in scale as Fig. 5a showing LSV characteristics of the produced films.

The heterostructure (WO_3/TiO_2–40 wt% film) showed a photocurrent density of 35.9 μA cm^{-2} at 0.75 V vs Ag/AgCl, which is higher than the photocurrent observed for WO_3 film. Additionally, the HE film presented a step increase above −0.24 V while for WO_3 film it is observed at approximately 0.1 V vs Ag/AgCl. It is usually assumed the onset potential where the water oxidation reaction takes place at the electrode film surface and it could be observed by the step increase in photocurrent, Fig. 5a. As a result, the WO_3/TiO_2–40 wt% film is showed to initiate water oxidation process at lower applied potentials as compared to WO_3 film. Indeed, the photoexcited electrons and holes generated at the electrode surface upon illumination occur at lower voltages for the

Table 2
Electrochemical characterization for the photocurrent density (J) using simulated solar irradiation at 50 mV s^{-1} and Na_2SO_4 0.5 mol L^{-1} at 0.75 V vs Ag/AgCl.

Samples	J ($\mu A\,cm^{-2}$)	J ($\mu A\,cm^{-2}$) with hole scavenger
Commercial TiO_2	–	12
WO_3	29.5	12
WO_3/TiO_2–40 wt%	35.9	210

heterostructured film and the negative shift of the onset potential represents a good response for photoelectrochemical water splitting.

For a better comprehension of the electronic mechanism in the photoelectrochemical cell, there are two main aspects to be considered: i) effective charge transport and ii) effective charge separation. By employing Na_2SO_3 0.5 mol L^{-1} + Na_2SO_4 0.5 mol L^{-1}, pH 6.0, the electrolyte (a hole scavenger) can completely suppress surface recombination without affecting charge separation within the space charge layer of the electrode. With this strategy we can differentiate between the two mechanisms that may be acting at the heterostructured material and to elucidate the electronic mechanism for water oxidation process. From Fig. 5b, WO_3/TiO_2–40 wt% film shows the best performance with 210 $\mu A\,cm^{-2}$ at 0.75 V vs Ag/AgCl. The isolated oxide films reached a photocurrent density of approximately 12 $\mu A\,cm^{-2}$ at the same conditions. Thus, the mechanism occurring on the heterostructured film is actually effective charge separation at the electrode surface, as indicated by the hole scavenger test in Fig. 5b. The increase in photocurrent density for the isolated oxide films in the presence of the hole scavenger is correlated to the decrease in surface charge recombination, since the sulfite electrolyte acts as a hole collector with 100% efficiency.

Apart from the hole scavenger test, the effect of the band edge alignment was investigated by Mott-Schottky plots, Fig. 6. It is assumed that for n-type semiconductors such as WO_3 and TiO_2, the difference between the flat band potential (E_{fb}) and the conduction band edge is very small [26]. Also, for a heterostructured system it is well established that electrons can flow from one semiconductor structure to another, when the Fermi level E_f of semiconductor $1 > E_f$ of semiconductor 2, until equilibrium is reached and E_f semiconductor 1 is similar to E_f semiconductor 2. Based on these statements, we can estimate the band energy levels for the produced films as a comparison with the observed photoelectrochemical performance for water oxidation.

According to Mott-Schottky plot (Fig. 6), the E_{fb} of TiO_2 is estimated as −1.34 and for WO_3 is −0.26 V vs Ag/AgCl. When the semiconductors are excited with appropriate light intensity, electrons can be transferred from the conduction band of TiO_2 to WO_3, since the E_{fb} of TiO_2 is 1.08 V higher than for WO_3, until thermodynamic equilibrium is established where E_f levels are the same across the heterojunction [27]. An opposite flow of holes (h^+) from the valence band of WO_3 to TiO_2 is expected. As a result, the photogenerated electrons and holes can be spatially distributed in two different crystalline phases of TiO_2 and WO_3 and charge recombination is inhibited, which can explain the efficient photocatalytic activity towards water oxidation in the photoelectrochemical cell, as compared to the performance of the isolated oxides [28]. This is in agreement with the hole scavenger test in Fig. 8b, where the increase in photocurrent density of WO_3/

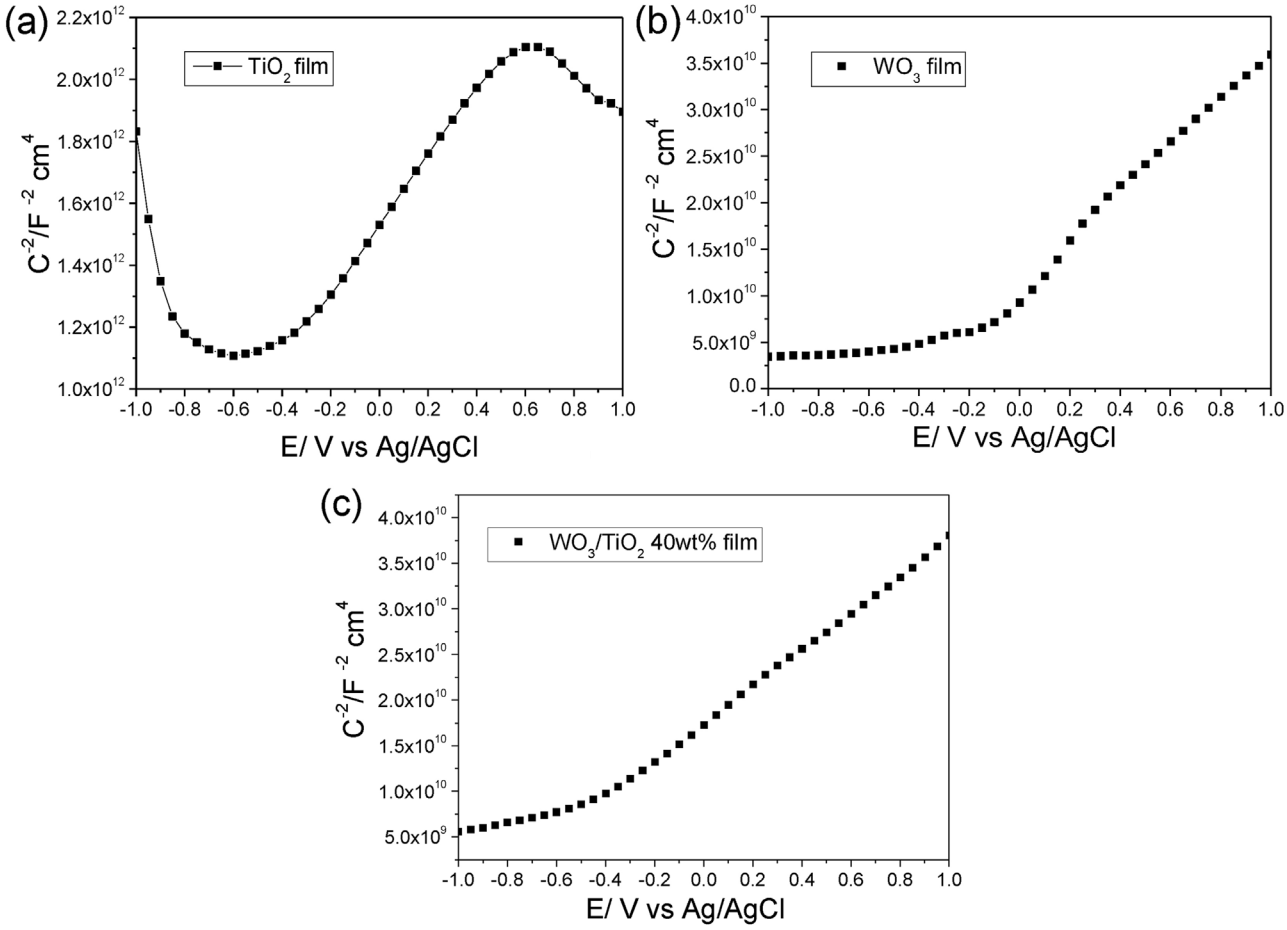

Fig. 6. Mott-Schottky plots without illumination at 10 kHz in 0.5 M Na_2SO_4 electrolyte. (a) TiO_2 film (b) WO_3 film and (c) WO_3/TiO_2–40 wt% film.

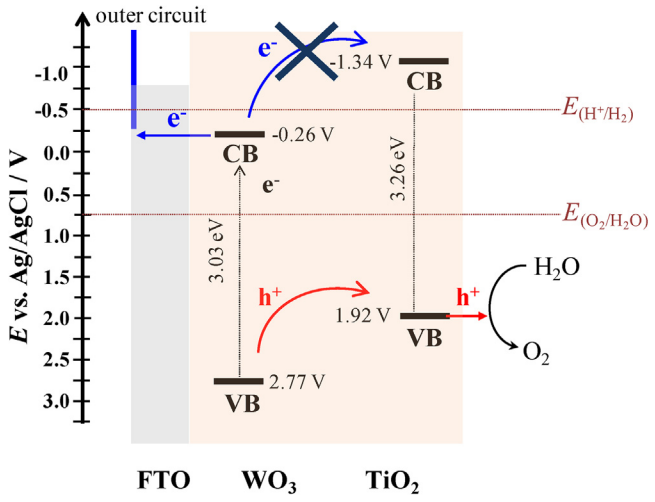

Fig. 7. Schematic band diagram of the WO_3/TiO_2 heterojunction photoanode for photoelectrochemical water oxidation.

TiO_2 40 wt% film is observed as a consequence of the effective charge separation mechanism and transference.

Also, it is possible to calculate the donor density (N_D) which is derived from Mott-Schottky plots as described elsewhere [19]. The films presented N_D values of 2.59×10^{18} and 1.17×10^{20} cm^3 for TiO_2 and WO_3 respectively. For the heterostructured film N_D is much higher (1.59×10^{20}) and it is in accordance to the best photoelectrochemical performance for water oxidation as exhibited by WO_3/TiO_2–40 wt% film.

To elucidate the band edge level for the films and to establish a correlation between heterojunction formation and enhanced photocurrent as observed through photocurrent-voltage measurements, the conduction band edge (E_{CB}) can be estimated with a small shift of the E_{fb} from the Mott Schottky plot [18]. The valence band edge (E_{VB}) can be determined with respect to E_{CB}, as $E_{VB} = E_{CB} + E_g$, where E_g is obtained by DRS analysis. The experimentally determined energy diagram is presented in Fig. 7. It is consistent with the formation of a type II heterostructure between TiO_2 and WO_3 and it correlates well to recent reports in the literature for the improvement of spatial charge separation and consequently increase in photocatalytic response [29,20]. Those results provide substantial arguments to explain the mechanisms that occur at the electrode surface for the photoassited water splitting.

When the heterostructure is illuminated with simulated solar irradiation, WO_3 is able to produce electron-hole pairs due to its electronic structure, where the holes at the E_{VB} of WO_3 are spontaneously injected into the E_{VB} of TiO_2 because of the work function and chemical potential difference between these semiconductors at the interface of a type II band alignment. On the other hand, the electrons at the E_{CB} of WO_3 are not allowed to be injected into the E_{CB} of TiO_2 due to thermodynamics as indicated in Fig. 6, which prevents charge recombination at the electrolyte solution and contributes to the migration of electrons to the outer circuit. Hence the WO_3/TiO_2 heterostruture is expected to exhibit the improved photocatalytic perforamance under simulated solar irradiation.

5. Conclusion

WO_3 and TiO_2 particles are in contact with each other, which show different particle morphologies of the heterostructures and the precursor oxides. The heterostructures were formed by the crystallization of WO_3 micro-particles attached to TiO_2 nanoparticles with agglomerate structure. The synthesis method as well as the deposition method is appropriate for the formation of WO_3:TiO_2 heterostructures due to the uniform distribution of Ti and W elements in the deposited film. Film preparation procedure was shown to influence phase composition of the heterostructures, where crystalline phase was not changed after film production for TiO_2 film (mainly anatase phase), but WO_3 changed from orthorhombic structure to hexagonal structure after calcination. WO_3/TiO_2–40 wt% film presented intermediate band gap energy (3.23 eV) between pristine TiO_2 (3.26 eV) and WO_3 values (3.03 eV). More evidence of the effective charge separation at the heterojuntion is showed using a hole scavenger during the photoelectrocatalytic tests where the photocurrent is much higher than the pure oxides (210 $\mu A\,cm^{-2}$ for the heterostructure and around 12 $\mu A\,cm^{-2}$ at 0.75 V vs Ag/AgCl for pure oxides). This is a clear evidence of heterostructures' photocatalytic efficiency toward water oxidation.

Acknowledgements

This work was supported by São Paulo Research Foundation—Brazil (FAPESP, grant 2015/16334-0). The authors thank Professor Ernesto Chavez Pereira for the facilities at the LIEC-UFSCar.

Appendix A. Supplementary data

Supplementary data associated with this article can be found, in the online version, at http://dx.doi.org/10.1016/j.jphotochem.2017.02.024.

References

[1] K. Nakata, A. Fujishima, TiO2 photocatalysis: design and applications, J. Photochem. Photobiol. C Photochem. Rev. 13 (2012) 169–189.
[2] S.Y. Lee, S.J. Park, TiO2 photocatalyst for water treatment applications, J. Ind. Eng. Chem. 19 (2013) 1761–1769, doi:http://dx.doi.org/10.1016/j.jiec.2013.07.012.
[3] H. Ali, N. Ismail, A. Hegazy, M. Mekewi, A novel photoelectrode from TiO2–WO3 nanoarrays grown on FTO for solar water splitting, Electrochim. Acta 150 (2014) 314–319.
[4] H. Zúñiga-benítez, G.A. Peñuela, Methylparaben removal using heterogeneous photocatalysis: effect of operational parameters and mineralization/biodegradability studies, Env. Sci Pollut. Res. (2016), doi:http://dx.doi.org/10.1007/s11356-016-6468-9.
[5] H. Zúñiga-benítez, G.A. Peñuela, Solar lab and pilot scale photo-oxidation of ethylparaben using H2O2 and TiO2 in aqueous solutions, J. Photochem. Photobiol. A Chem. 337 (2017) 62–70, doi:http://dx.doi.org/10.1016/j.jphotochem.2017.01.019.
[6] Henry Zúniga-Benítez, C. Aristizabal-Ciro, G.A. Penuela, Heterogeneous photocatalytic degradation of the endocrine–disrupting chemical benzophenone-3: parameters optimization and by-products identification, J. Environ. Manag. 167 (2016) 246–258, doi:http://dx.doi.org/10.1016/j.jenvman.2015.11.047.
[7] M. Anpo, Photocatalytic reduction of CO2 with H2O on highly dispersed Ti-oxide catalysts as a model of artificial photosynthesis, J. CO2 Util. 1 (2013) 8–17.
[8] K. Shen, K. Wu, D. Wang, Band alignment of ultra-thin hetero-structure ZnO/TiO2 junction, Mater. Res. Bull. 51 (2014) 141–144, doi:http://dx.doi.org/10.1016/j.materresbull.2013.12.013.
[9] V. Pfeifer, P. Erhart, S. Li, K. Rachut, J. Morasch, J. Brötz, P. Reckers, T. Mayer, S. Rühle, A. Zaban, I. Mora Seró, J. Bisquert, W. Jaegermann, A. Klein, Energy band alignment between anatase and rutile TiO_2, J. Phys. Chem. Lett. 4 (2013) 4182–4187, doi:http://dx.doi.org/10.1021/jz402165b.
[10] X. Shi, I. Herraiz-cardona, L. Bertoluzzi, P. Lopez-varo, J. Bisquert, J.H. Park, S. Gimenez, Understanding the synergistic effect of WO3-BiVO4 heterostructures by impedance spectroscopy, Phys. Chem. Chem. Phys. 18 (2016) 9255–9261, doi:http://dx.doi.org/10.1039/C5CP07905E.
[11] L. Yang, H. Zhou, T. Fan, D. Zhang, Semiconductor photocatalysts for water oxidation: current status and challenges, Phys. Chem. Chem. Phys. 16 (2014) 6810–6826, doi:http://dx.doi.org/10.1039/c4cp00246f.
[12] I.A. de Castro, J.A. de Oliveira, E. Cristina, T. Giraldi, C. Ribeiro, Production of heterostructured TiO2/WO3 Nanoparticulated photocatalysts through a simple one pot method, Ceram. Int. 41 (2015) 3502–3510.
[13] P. Dias, T. Lopes, L. Meda, L. Andrade, A. Mendes, Photoelectrochemical water splitting using WO3 photoanodes: the substrate and temperature, Phys. Chem. Chem. Phys. 18 (2016) 5232–5243, doi:http://dx.doi.org/10.1039/C5CP06851G.

[14] X. Liu, F. Wang, Q. Wang, Nanostructure-based WO3 photoanodes for photoelectrochemical water splitting, Phys. Chem. Chem. Phys. 14 (2012) 7894–7911, doi:http://dx.doi.org/10.1039/c2cp40976c.
[15] J. Zhang, Z. Liu, Z. Liu, Novel WO3/Sb2S3 heterojunction photocatalyst based on WO3 of different morphologies for enhanced efficiency in photoelectrochemical water splitting, Appl. Mater. Interfaces 8 (2016) 9684–9691, doi:http://dx.doi.org/10.1021/acsami.6b00429.
[16] X. Zhang, Y. Wang, B. Liu, Y. Sang, H. Liu, Heterostructures construction on TiO2 nanobelts: a powerful tool for building high-performance photocatalysts, Appl. Catal. B Environ. 202 (2017) 620–641, doi:http://dx.doi.org/10.1016/j.apcatb.2016.09.068.
[17] I.A. de Castro, W. Avansi, C. Ribeiro, WO3/TiO2 heterostructures tailored by the oriented attachment mechanism: insights from their photocatalytic properties, CrystEngComm (2014), doi:http://dx.doi.org/10.1039/c3ce41668b.
[18] R. Beranek, (Photo)electrochemical methods for the determination of the band edge positions of TiO2-based nanomaterials, Adv. Phys. Chem. 2011 (2011) 1–20, doi:http://dx.doi.org/10.1155/2011/786759.
[19] R.G. Freitas, M.A. Santanna, E.C. Pereira, Preparation and characterization of TiO2 nanotube arrays in ionic liquid for water splitting, Electrochim. Acta 136 (2014) 404–411, doi:http://dx.doi.org/10.1016/j.electacta.2014.05.097.
[20] I.A. de Castro, W. Avansi, C. Ribeiro, WO3/TiO2 heterostructures tailored by the oriented attachment mechanism: insights from their photocatalytic properties, CrystEngComm 16 (2014) 1514, doi:http://dx.doi.org/10.1039/c3ce41668b.
[21] V.R. de Mendonça, C.J. Dalmaschio, E.R. Leite, M. Niederberger, C. Ribeiro, Heterostructure formation from hydrothermal annealing of preformed nanocrystals, J. Mater. Chem. A 3 (2015) 2216–2225, doi:http://dx.doi.org/10.1039/C4TA05926C.
[22] J. Zhang, L. Huang, Z. Lu, Z. Jin, X. Wang, G. Xu, E. Zhang, H. Wang, Z. Kong, J. Xi, Z. Ji, Crystal face regulating MoS2/TiO2 (001) heterostructure for high photocatalytic activity, J. Alloys Compd. 688 (2016) 840–848, doi:http://dx.doi.org/10.1016/j.jallcom.2016.07.263.
[23] P. Kundu, E. a Anumol, C. Nethravathi, N. Ravishankar, Existing and emerging strategies for the synthesis of nanoscale heterostructures, Phys. Chem. Chem. Phys. 13 (2011) 19256–19269, doi:http://dx.doi.org/10.1039/c1cp22343g.
[24] J. Li, J. Huang, J. Wu, L. Cao, Q. Li, K. Yanagisawa, Microwave-assisted growth of WO3·0.33H2O micro/nanostructures with enhanced visible light photocatalytic properties, CrystEngComm 15 (2013) 7904, doi:http://dx.doi.org/10.1039/c3ce41005f.
[25] C.V. Ramana, S. Utsunomiya, R.C. Ewing, C.M. Julien, U. Becker, Structural stability and phase transitions in WO3 thin films, J. Phys. Chem. B 110 (2006) 10430–10435, doi:http://dx.doi.org/10.1021/jp056664i.
[26] G. Zhang, D. Monllor-Satoca, W. Choi, Band energy levels and compositions of CdS-based solid solution and their relation with photocatalytic activities, Catal. Sci. Technol. 3 (2013) 1790–1797, doi:http://dx.doi.org/10.1039/c3cy00066d.
[27] T. Uddin, Y. Nicolas, T. Toupance, M.M. Mu, H. Kleebe, K. Rachut, J. Ziegler, A. Klein, W. Jaegermann, Preparation of RuO2/TiO2 mesoporous heterostructures and rationalization of their enhanced photocatalytic properties by band alignment investigations, J. Phys. Chem. C 117 (2013) 22098–22110.
[28] M. Ju, G. Sun, J. Wang, Q. Meng, W. Liang, Origin of high photocatalytic properties in the mixed-phase TiO2: a first-principles theoretical study, Appl. Mater. Interfaces 6 (2014) 12885–12892.
[29] J. Yang, X. Zhang, H. Liu, C. Wang, S. Liu, P. Sun, L. Wang, Y. Liu, Heterostructured TiO2/WO3 porous microspheres: preparation, characterization and photocatalytic properties, Catal. Today 201 (2013) 195–202, doi:http://dx.doi.org/10.1016/j.cattod.2012.03.008.